Sensors and Materials, Vol. 38, No. 11 (2026) 6595–6620
MYU Tokyo

S & M 4697

Elite-preserving Two-stage Red-billed Blue Magpie Optimization for Coordinated Photovoltaic and Battery Energy Storage Planning and Operation in Distribution Networks

Zirui Zhang,[1] Yinglei Dong,[1] Lingling Li,[2] and Haojie Zhu[2*]

[1]School of International Education, Hebei University of Technology, Tianjin 300401, China
[2]School of Electronic and Information Engineering, Hebei University of Technology, Tianjin 300401, China

(Received September 1, 2026; accepted November 9, 2026)

Keywords: photovoltaic generation, battery energy storage, coordinated planning and operation, elite preservation, red-billed blue magpie optimizer

The configuration and operation of the photovoltaic (PV) generation and battery energy storage system (BESS) are closely related, and the locations and capacities of the equipment directly affect the hourly operation of the battery. In this study, a two-stage optimization framework combining a seven-variable planning search, a 24-variable operation search, a common repaired objective, and an inter-stage elite acceptance mechanism is constructed using the original red-billed blue magpie optimizer (RBMO). Measured load and PV profiles are employed as sensor-derived inputs, while voltage and state of charge are obtained from the models. The IEEE 33-bus system is selected as a case study, and three methods are compared under an equal evaluation budget with 30 runs for each method. The results show that the mean penalized objective values obtained by the single-stage RBMO and the elite two-stage framework are 0.685268 and 0.653401, respectively. The elite acceptance mechanism prevents the deterioration of the retained state, but its final-objective difference from the two-stage method without elite acceptance is not statistically significant. In addition, seven weight settings and five scaled load/PV conditions are analyzed to examine the objective trade-offs, storage capacities, and transfer of nominal configurations. Under low load and high PV, replanning obtains 30 feasible results, while no feasible result is obtained for the fixed nominal configurations within the tested redispatch budget. Therefore, the framework provides a coordinated search procedure and transparent assessment, but a single-day configuration does not ensure feasibility under different operating conditions, and correlated multi-day data and uncertainty-aware planning are still required for practical application.

1. Introduction

The increasing penetration of photovoltaic (PV) generation changes the magnitude and temporal distribution of power flow in distribution networks. Since PV output depends on irradiance rather than load demand, the unreasonable coordination of PV installations may result

*Corresponding author: e-mail: 202511901013@stu.hebut.edu.cn
https://doi.org/10.18494/SAM6604

ISSN 0914-4935 © MYU K.K.

in reverse power flow, voltage rise, voltage-limit violations, and additional network losses.[1–4] Therefore, the locations, installed capacities, and daily relationship between load demand and PV generation need to be considered in PV planning, rather than evaluating the installed capacity alone.

A battery energy storage system (BESS) can improve the matching of PV generation and load demand through energy shifting, peak shaving, and voltage support, and its operational benefits depend on both the installation location and operation scheme. Reasonable BESS siting and sizing can reduce network losses, voltage deviation, and peak demand,[5,6] while state-of-charge (SOC) management affects the economic and network benefits obtained from the battery.[3,7] Therefore, whether the configured battery can be effectively utilized depends on the coordination between its hourly operation scheme and the planning decision, rather than on capacity selection alone.

Different planning-operation structures have been employed to describe the coupling between equipment configuration and operation. Chedid and Sawwas applied a two-step approach to PV-storage planning,[8] and Thokar *et al.* constructed a nested multi-objective framework for simultaneous installations.[9] Elseify *et al.* investigated probabilistic planning with time-varying loads and subsequently analyzed scheduling under different loading scenarios.[10,11] Reliability-oriented, life-cycle, and demand-response studies extended the objectives of the planning model,[12–14] while the master–slave strategy and coordinated lifetime/reliability optimization provided different methods for organizing planning and operating decisions.[15,16] In addition, dynamic thermal rating was introduced to improve network flexibility.[17] The above studies demonstrate the importance of coordinated decisions. On this basis, the present study focuses on retaining a complete accepted state when a stochastic optimization stage with a finite search budget produces an inferior candidate.

Metaheuristic outputs are also random samples rather than deterministic answers. Repeated runs and comparable computational budgets are therefore needed for a meaningful comparison.[18,19] In the preliminary joint search used here, RBMO occasionally found a good solution but showed a large run-to-run variation, which motivated a search structure that controls both variable coupling and inter-stage degradation.

The red-billed blue magpie optimizer (RBMO) was proposed by Fu *et al*.,[20] which performs optimization by simulating searching, attacking, and food-storage behaviors. In this study, the original RBMO update rules are retained, and a planning-operation framework with an additional elite acceptance mechanism is constructed to determine whether the complete output of a stage can replace the accepted state. Therefore, the contribution lies in the RBMO-based coordination framework, rather than in a new population-update variant. The information flow of the framework is shown in Fig. 1.

The framework conducts stochastic, inexact alternating optimization, in which one variable block is optimized while the other block remains fixed, and the obtained candidate is subsequently evaluated by the complete-objective acceptance test. This procedure is related to block-coordinate optimization.[21] However, the finite RBMO subproblems, discrete bus decisions, and repair procedure do not satisfy a general guarantee of exact coordinate minimization. Therefore, stationary-point or global convergence is not claimed, and the

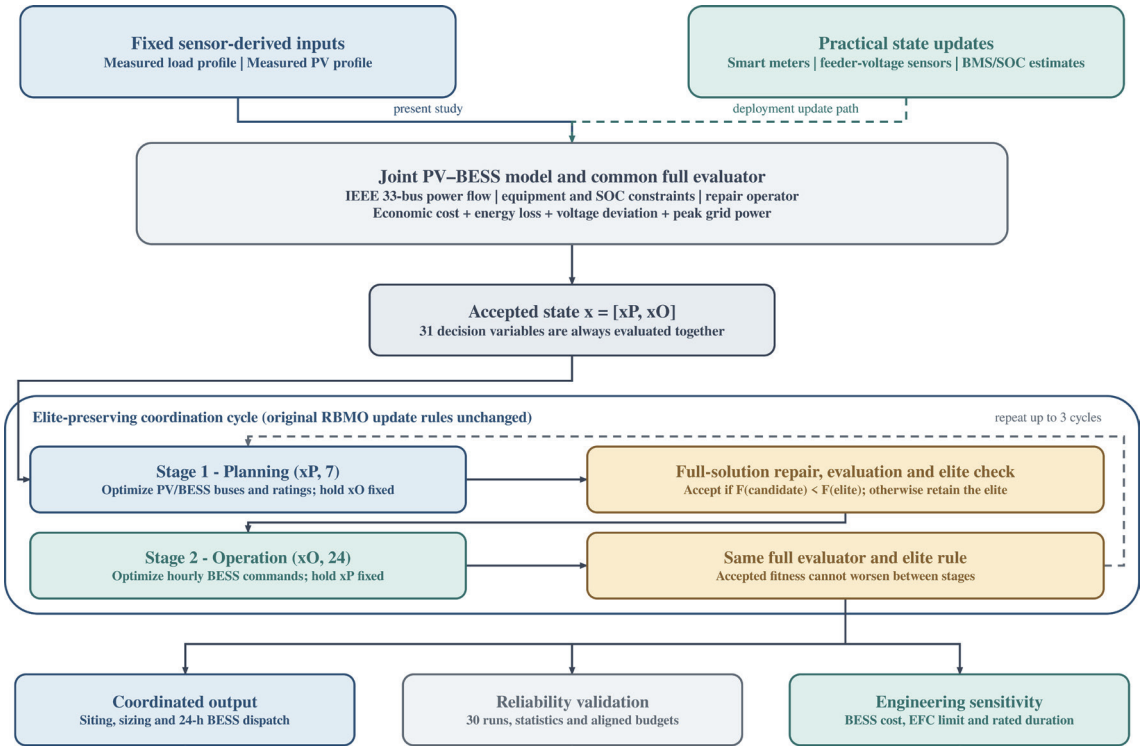

Fig. 1. (Color online) Information flow of the planning-operation framework. The stage outputs are evaluated by a common repaired objective before updating the shared state, and three coordination cycles are employed in the revised formal experiments.

contribution of this study is the integration of these procedures and the evidence obtained in the PV-BESS application.

In this study, the two stages refer to the alternating optimization of planning and operation variables, rather than two-stage robust optimization. The model does not introduce an uncertainty set, a worst-case adversary, a min-max-min formulation, or column-and-constraint generation. The additional scenarios are employed for deterministic stress tests and do not constitute a robust counterpart.

The main contribution of this study is the integration of planning-operation decomposition, a common repaired evaluator, and a stage-level elite acceptance mechanism for coordinated PV-BESS siting, sizing, and scheduling. Alternating updates and elitist acceptance are existing optimization methods and are not proposed as new general principles in this study. To analyze their individual effects, three methods are compared through an equal-budget ablation experiment. Moreover, objective-weight sensitivity and fixed-configuration scenario tests are conducted to examine the limitations of the obtained configuration schemes.

The measured load and PV profiles are employed as optimization inputs, providing the relation between this study and sensing applications. In practical deployment, smart meters and PV monitors would be used to update these inputs, while feeder-voltage sensors and battery management system (BMS) SOC estimates would provide information for operating-state

assessment. The planning and scheduling model is evaluated offline in this study, and field sensor validation is not conducted.

2. System Modeling and Problem Formulation

2.1 Distribution network and representative daily scenario

The IEEE 33-bus radial system is used as the test network.[22] Bus 1 is the slack bus and buses 2–33 are candidate PV/BESS locations. A backward-forward sweep calculates hourly power flow. Under the original peak load, the model gives 202.677 kW active loss, 0.913090 p.u. minimum voltage, and 3917.677 kW slack power, consistent with the standard system results.[22]

A representative spring day is constructed from the measured data. The load shape uses the March 2023 one-minute records of Tianjin, averaged by time of day and normalized by its daily maximum; the PV shape uses the PV column of the 5 April 2022 renewable dataset and is processed in the same way. Since the two datasets are not synchronized, they describe representative temporal shapes rather than one historical PV-load day. This limitation is kept in the interpretation of the results. The measured load and PV records are treated as sensor-derived profiles, whereas voltage and SOC are obtained from the network and battery models.

In a practical sensing architecture, smart-meter active-power measurements would be used to update the load estimates, PV monitoring would update the generation profiles, feeder voltage sensors would support state assessment, and a battery management system (BMS) would provide SOC estimates. In this study, archived load/PV records are employed, and voltage and SOC are calculated using the models. Therefore, the results do not constitute the validation of a sensor, sensing material, online state estimator or field control installation.

For bus i and hour t, the active net load is

$$P_{i,t}^{net} = \lambda_t P_i^{load} - P_{i,t}^{PV} - P_{i,t}^{B}, \tag{1}$$

where the original bus load is scaled by the hourly load factor. PV output and BESS discharge reduce net demand; negative BESS power represents charging.

2.2 PV generation model

Two PV units are optimized. For unit k, the hourly active output is

$$P_{k,t}^{PV} = S_k^{PV} \phi_t, \tag{2}$$

where the rated PV capacity is multiplied by the normalized PV profile. Candidate buses are 2–33 and each unit is limited to 100–2500 kW.

PV follows the given active-power profile; curtailment and inverter reactive-power control

are not included. This keeps the study focused on active-power planning and storage scheduling, although these functions can be added in a later model.

2.3 BESS model and operating constraints

The decision variables of the BESS include the installation bus, rated energy E_B, rated power P_B, and 24 normalized commands u_t. Before sequential SOC repair, the requested battery power can be expressed as

$$P_t^B = u_t P_B. \tag{3}$$

Positive battery power represents discharge, whereas negative battery power represents charging. Since sequential SOC repair may reduce the requested power, the actual repaired trajectory is employed to calculate the SOC update, economic terms, cycling index, and network performance.

SOC is updated sequentially with charging and discharging efficiencies of 0.95:

$$SOC_t = SOC_{t-1} + \frac{\eta_{ch} P_t^{ch} \Delta t}{E_B} - \frac{P_t^{dis} \Delta t}{\eta_{dis} E_B}. \tag{4}$$

The initial SOC is 0.50 and is restricted to 0.20–0.90; the terminal value must return within 0.005 of the initial SOC so that a one-day solution cannot gain benefit by simply emptying the battery.

The nominal storage duration is defined by

$$T_B = \frac{E_B}{P_B}. \tag{5}$$

The daily use of the battery is further restricted by the equivalent full cycle (EFC) index, which is expressed as

$$EFC = \frac{\sum_{t=1}^{24} \left(P_t^{ch} + P_t^{dis} \right) \Delta t}{2E_B} \le EFC_{max} \tag{6}$$

with a base limit of 1.0. The EFC constraint is a simplified cycling restriction rather than a complete electrochemical aging model.

2.4 Economic model

The daily economic objective is constructed by considering grid-energy cost, maximum-demand cost, the annualized investment of PV and BESS, operation and maintenance (O&M), and battery-throughput degradation, which can be expressed as

$$C_{eco} = C_{grid} + C_{peak} + C_{PV} + C_{BESS} + C_{deg}. \tag{7}$$

Grid-energy cost is calculated from hourly import and the time-of-use tariff:

$$C_{grid} = \sum_{t=1}^{24} \rho_t P_t^{grid} \Delta t. \tag{8}$$

Peak, flat, and valley prices are 0.954768, 0.668468, and 0.359268 CNY/kWh, respectively. Valley hours are 23:00–07:00; flat hours are 07:00–09:00, 12:00–16:00, and 21:00–23:00; the remaining hours are peak periods.

The maximum-demand cost is

$$C_{peak} = c_{dem} \max_t \left(P_t^{grid} \right) \tag{9}$$

using a daily demand price of 1.34194 CNY/(kW day), converted from 41.6 CNY/(kW month). Investment is annualized with the capital recovery factor

$$CRF\left(r,n\right) = \frac{r\left(1+r\right)^n}{\left(1+r\right)^n - 1}. \tag{10}$$

The daily PV cost is

$$C_{PV} = \frac{c_{PV} \sum_k S_k^{PV} \left[CRF\left(r, n_{PV}\right) + m_{PV} \right]}{365}, \tag{11}$$

where the PV capital expenditure (CAPEX) is set to 3200 CNY/kW, the service life is set to 20 years, and the annual O&M is set to 1%.

The BESS investment term is

$$C_{BESS} = \frac{\left(c_E E_B + c_P P_B\right)\left[CRF\left(r, n_B\right) + m_B \right]}{365}, \tag{12}$$

with 1000 CNY/kWh energy cost, 500 CNY/kW power cost, 10-year life, and 1.5% annual O&M.

Detailed battery aging depends on SOC, depth of discharge, temperature, and calendar effects.[23] Because these data are outside the present planning model, degradation is represented by a linear throughput charge:

$$C_{deg} = c_{deg} \sum_{t=1}^{24} \left(P_t^{ch} + P_t^{dis} \right) \Delta t. \tag{13}$$

The coefficient is 0.10 CNY/kWh throughput. Its purpose is to penalize unnecessary cycling, while the sensitivity analysis tests the effect of the broader storage assumptions.

2.5 Distribution-network performance indices

Three network indices are added to economic cost. The daily active energy loss is

$$E_{loss} = \sum_{t=1}^{24} P_{loss,t} \Delta t. \tag{14}$$

The accumulated voltage-deviation index is

$$VD = \sum_{t=1}^{24} \sum_{i=2}^{33} \left| 1 - V_{i,t} \right| \cdot \tag{15}$$

The peak upstream-grid power is

$$P_{peak} = \max_t \left(P_t^{grid} \right). \tag{16}$$

These indices represent network efficiency, overall voltage condition, and upstream capacity use. Since storage actions can improve one index while worsening another, they are evaluated together.

2.6 Normalized objective function and constraints

The four components have different units, so they are normalized by the corresponding Base-case values. The complete fitness is

$$F = 0.55 \frac{C_{eco}}{C_0} + 0.15 \frac{E_{loss}}{E_{loss,0}} + 0.15 \frac{VD}{VD_0} + 0.15 \frac{P_{peak}}{P_{peak,0}} + Pen. \tag{17}$$

The weight of economic cost is set to 0.55, and the weights of network loss, accumulated voltage deviation, and peak grid power are each set to 0.15. The baseline setting gives a majority share to economic cost while retaining the three network objectives, which represents an illustrative cost-oriented planning preference. However, the weights are not calibrated stakeholder utilities and are not claimed to be objectively optimal. To analyze the impact of weight selection, seven settings are examined in Sects. 4.8 and 5.5. Equation (17) presents the baseline objective, and its four coefficients are replaced by the corresponding values for each sensitivity setting.

All candidates are also checked against voltage, SOC, terminal SOC, duration, EFC, equipment bounds, power-flow convergence, and zero grid-export requirements. The voltage and import constraints are enforced as 0.90-1.05 p.u. and non-negative grid power, respectively; remaining violations after repair receive penalties. Thus, the same complete evaluator is used in both optimization stages and in all benchmark methods.

3. Inter-stage Elite-preserving Two-stage RBMO Framework

3.1 Original joint decision space

The complete decision vector is

$$x = \left[b_{PV1}, b_{PV2}, b_B, S_{PV1}, S_{PV2}, E_B, P_B, u_1, \ldots, u_{24}\right]. \tag{18}$$

The complete decision vector consists of three device buses, two PV capacities, the BESS energy and power ratings, and 24 hourly battery commands. The first seven variables are integrated as the planning vector x^P, while the remaining 24 variables constitute the operation vector x^O.

In the following text, E_B and P_B represent the rated energy and power of the BESS, respectively; P_t^B represents the actual hourly battery power; SOC_t represents the modeled state of charge; and EFC represents the daily equivalent full cycles. The planning and operation vectors are denoted by x^P and x^O, respectively, and are combined to form the complete vector in the order given in Eq. (18).

A direct 31-dimensional search mixes discrete buses, continuous capacities, and time-coupled operating variables. Since changing the BESS size changes the feasible SOC trajectory, a schedule that is reasonable for one plan may be poor for another. The two-stage method therefore changes the search organization, not the physical model: each partial candidate is always reconstructed and evaluated as a complete solution.

3.2 RBMO optimization engine

The original RBMO of Fu *et al.*[20] is used without changing its population initialization, searching, attacking, or food-storage rules. RBMO first explores with group-based search and then concentrates around the current food position; its internal food-storage rule retains the

better individual after an update. Because these equations are unchanged from the original algorithm, they are not repeated here. The modification in this study is only the coordination structure outside each RBMO call.

The framework does not introduce local-search escape operators, population-diversity control, or adaptive RBMO parameters. The decomposition changes the dimension of each optimization call, while the stage acceptance mechanism retains the shared state. However, these two procedures do not independently demonstrate that premature convergence or exploration-exploitation imbalance has been resolved. Therefore, repeated-run results and rejected-stage records are employed to describe the observed behavior, and a population-level mechanism that has not been measured is not claimed.

3.3 Framework overview

Each coordination cycle starts from one accepted complete planning-operation state. Although a stage searches only part of the variables, acceptance is based on the full repaired objective.

Let $R(.)$ denote the common repair operator. The evaluator used by both stages is

$$\tilde{F}(x) = F(R(x)). \tag{19}$$

The repair procedure first rounds the bus variables, restricts the equipment ratings, enforces the storage energy-to-power ratio, and limits the actual hourly battery power through sequential SOC updates. Then, terminal SOC, EFC, voltage, export, and power-flow convergence are evaluated, and penalties are imposed on the remaining violations. The same duration repair is applied to the three methods in the formal ablation experiment, and the sensor-derived profiles remain fixed during each optimization run.

3.4 Stage 1: Planning optimization

Stage 1 fixes the accepted operation vector and searches the seven planning variables. Its objective is

$$f_P\left(\boldsymbol{x}^P \middle| \boldsymbol{x}^{O,elite}\right) = F\left(R\left[\boldsymbol{x}^P, \boldsymbol{x}^{O,elite}\right]\right). \tag{20}$$

Each planning candidate is combined with the fixed 24-hour schedule and then repaired. Therefore, BESS power and SOC are recalculated when the energy or power rating changes rather than copied from the previous plan.

Stage 1 uses 30 individuals and 100 RBMO iterations.

3.5 Stage 2: Operation optimization

Stage 2 fixes the accepted planning vector and optimizes the 24-hour battery commands. Its objective is

$$f_O\left(x^O \middle| x^{P,elite}\right) = F\left(R\left(\left[x^{P,elite}, x^O\right]\right)\right). \tag{21}$$

SOC is checked sequentially from hour 1 to 24, and any command exceeding an SOC boundary is reduced to the feasible value. Terminal SOC, EFC, and network constraints are then evaluated by the same full objective.

Because capacities and locations remain fixed, Stage 2 can focus on the timing of price, load, PV output, and battery operation; however, it does not optimize arbitrage alone because losses, voltage, and peak power remain in the objective. Stage 2 uses 40 individuals and 150 iterations.

3.6 Inter-stage elite acceptance and rejection

A complete stage can return a worse stochastic candidate. To prevent this candidate from becoming the next starting state, Stages 1 and 2 both use the following acceptance rule:

For candidate x_{cand} with fitness F_{cand}, the accepted state is updated by

$$\left(\boldsymbol{x}^{elite}, F^{elite}\right) \leftarrow \begin{cases} \left(\boldsymbol{x}^{cand}, F^{cand}\right), & F^{cand} < F^{elite} - \varepsilon, \\ \left(\boldsymbol{x}^{elite}, F^{elite}\right), & \text{otherwise.} \end{cases} \tag{22}$$

When the candidate does not improve the accepted objective by more than the tolerance of 10^{-10}, the candidate is rejected. The inter-stage elite acceptance mechanism is different from the food-storage mechanism of RBMO: food storage is applied within an optimizer call, while inter-stage acceptance compares complete solutions obtained after a full planning or operation stage.

The accepted penalized objective does not increase at the stage boundaries, indicating that the mechanism can retain the quality of the shared state. However, this property does not ensure global optimality, population diversity, escape from local optima, or strict feasibility. Since the acceptance decision is based on the weighted objective and penalties rather than a feasibility-first ordering, the selected candidate does not necessarily have the smallest constraint violation.

3.7 Initialization, repair, and termination

The initial schedule is price-based: the eight lowest-price hours receive light charging commands and the eight highest-price hours receive discharging commands. It is then repaired before optimization. This reduces severe initial SOC violations, while Stage 2 remains free to change every hourly command.

Repair is applied in a fixed order: device buses and ratings are bounded, the energy-to-power ratio is checked, normalized commands are converted to actual power, SOC violations are repaired sequentially, and terminal SOC, EFC, voltage, export, and power-flow conditions are evaluated. Unresolved violations receive penalties.

To maintain the same search budget for each run, exactly three coordination cycles are employed in the revised ablation, weight, and scenario-replanning experiments. In the earlier optimizer comparison, the maximum number of cycles was set to three, the relative-improvement tolerance was set to 10^{-4}, and the no-improvement patience was set to two cycles. All reported formal runs in that comparison reached the cycle limit.

The workflow is therefore concise: initialize and repair a complete state, optimize planning, accept only an improved complete candidate, optimize operation, apply the same acceptance rule, and finally re-evaluate the retained elite with the full 31-dimensional objective.

3.8 Objective-function evaluations and computational cost

Each iteration of RBMO evaluates both a searching update and an attacking update. Therefore, the number of search evaluations in Stage 1 is 30 + 2(30)(100) = 6030, while that in Stage 2 is 40 + 2(40)(150) = 12040. The total search budget for three cycles is 54210, which is adopted in each run of the revised ablation, weight, and scenario-replanning experiments. In the earlier four-optimizer comparison, the additional initialization and verification calls were included, giving approximately 54219 complete evaluations. The two evaluation-accounting conventions are therefore reported separately.

The expensive part is the complete objective because every candidate requires 24 hourly power-flow calculations. Therefore, the optimizer comparison is aligned by objective-function evaluations rather than the raw number of iterations.

In the historical comparison, particle swarm optimization (PSO), the grey wolf optimizer (GWO), and the genetic algorithm (GA) employ 200 planning iterations and 300 operation iterations. This setting provides the same search-evaluation budget, while the decomposition procedure, repair method, and elite acceptance rules remain consistent among the algorithms.

4. Case Study and Experimental Design

4.1 Case-study system and input data

The case study uses the IEEE 33-bus system and the sensor-derived representative profiles defined in Sect. 2. The original spatial load distribution is retained while all buses follow the same hourly load factor. PV output and the time-of-use tariff create both daytime and evening operating conflicts, so BESS can perform price shifting, PV shifting, and peak reduction. Since the load and PV records are not synchronized, the case is interpreted as a representative spring day rather than an annual operating forecast.

The main parameters are listed in Table 1. Equipment costs and lifetimes are planning assumptions rather than market forecasts; storage cost is therefore examined again in the sensitivity study.

4.2 Engineering comparison cases

Three engineering cases are compared. Case 1 is the Base system without PV or BESS and provides the normalization values. Case 2 optimizes two PV buses and capacities with BESS removed. Case 3 uses the complete two-stage PV-BESS model. The Base comparison measures the total effect of PV-BESS, whereas the PV-only comparison isolates the additional value of storage. The reported indicators include fitness, economic cost, grid energy, loss, peak power, voltage deviation, minimum voltage, and equipment size.

4.3 Equal-budget decomposition and elite ablation

To analyze the effects of decomposition and elite acceptance, the direct single-stage RBMO, the two-stage RBMO without inter-stage elite acceptance, and the two-stage RBMO with elite acceptance are selected for the formal ablation experiment. Each method is executed 30 times with matched seed identifiers, the same complete evaluator, and the same equipment, duration, and SOC repair procedures. For the single-stage RBMO, the population size and the number of iterations are set to 30 and 903, respectively, giving $30 + 2(30)(903) = 54210$ search evaluations. For the two two-stage methods, the settings described in Sect. 3 are employed for three cycles, also giving 54210 evaluations. When elite acceptance is removed, every candidate returned by a stage replaces the shared state, and the final and historical best states are recorded separately.

Table 1
Principal model parameters.

Parameter	Value
Candidate buses	2–33
Number of PV units	2
Capacity of each PV unit	100–2500 kW
BESS energy	200–3000 kWh
BESS power	100–1000 kW
BESS duration	2–6 h
Initial SOC	0.50
SOC range	0.20–0.90
Terminal SOC tolerance	0.005
Charging/discharging efficiency	0.95/0.95
Base daily EFC limit	1.0
Voltage range	0.90–1.05 p.u.
Grid export	Not allowed
Discount rate	5%
PV lifetime	20 years
BESS lifetime	10 years
Objective weights	0.55/0.15/0.15/0.15

The equal-budget ablation experiment is employed as the main evidence for assessing the framework, replacing the earlier single-stage comparison with an unequal budget. The earlier single-stage budget tests are retained as diagnostic experiments and are not used to quantify the individual effects of decomposition and elite acceptance. Matched seed identifiers are employed for paired comparisons, but different acceptance paths may change the consumption of random numbers, so identical stage candidates are not necessarily obtained.

4.4 Success criterion and repeated-run design

The three methods in the revised ablation experiment are each executed with 30 matched-seed runs, and each of the seven objective-weight settings is also executed 30 times. In the scenario experiments, 30 nominal configurations are assessed under five operating conditions. The original 30-run designs are retained for the historical PV-only and four-optimizer studies. Reused baseline results are identified separately and are not counted as new independent observations.

The best PV-only fitness of 0.661696 is retained as the reference threshold to maintain consistency with the original engineering comparison. A run is considered successful only when the final objective is below this threshold and the solution is numerically feasible. This criterion is different from obtaining an objective below the no-equipment Base value of 1.0. Therefore, threshold successes and feasible counts are reported separately in the revised ablation experiment.

A solution is classified as numerically feasible when the power flow converges and every recorded residual constraint violation is no greater than 10^{-7}. The terminal-SOC residual is calculated beyond the prescribed return tolerance of 0.005, while the EFC residual is calculated above the imposed daily limit. The same criterion is applied to small residuals without changing the classification rule. In addition, runtime is employed for an internal implementation comparison, rather than as a hardware-independent measure of algorithm complexity.

4.5 Optimizer comparison under aligned evaluation budgets

RBMO, PSO, GWO, and GA use the same two-stage framework, variables, repair, objective, initial scenario, elite rule, and cycle limit; only the population-update mechanism differs.

Equal iteration counts would be misleading because RBMO evaluates the population twice per iteration, whereas the implemented PSO, GWO, and GA perform approximately one population evaluation. Their number of iterations are therefore increased to align the expensive objective-evaluation budget, as summarized in Table 2.

The resulting budget is approximately 54,219 complete evaluations per run for each method. This does not make the algorithms mathematically identical, but it controls the dominant workload more directly than the equal number of iterations.[19]

Table 2
Optimizer settings under aligned objective-function evaluation budgets.

Optimizer	Stage 1 population	Stage 1 iterations	Stage 2 population	Stage 2 iterations	Approximate evaluations per run
RBMO	30	100	40	150	54219
PSO	30	200	40	300	54219
GWO	30	200	40	300	54219
GA	30	200	40	300	54219

4.6 Statistical analysis

For the historical four-optimizer comparison, the original Kruskal-Wallis test, Mann-Whitney U test, Holm correction, and Cliff effect-size analysis are retained. For the revised ablation experiment, two-sided exact paired sign tests are employed to compare the final penalized and historical-best penalized objectives, with the tie tolerance set to 10^{-10}. Holm correction is applied to all six tests, which consist of three method pairs and two endpoints. Moreover, feasible counts and feasible-only descriptive statistics are reported separately. Infeasible runs are not removed before the paired tests, since their removal would change the paired sample.

4.7 Sensitivity-analysis design

Three sensitivity groups are used because the base best solution reaches the minimum duration and daily EFC limits, while the BESS cost is an important planning assumption.

4.7.1 BESS investment cost

BESS energy and power CAPEX are multiplied together by 0.6, 0.8, 1.0, 1.2, and 1.4, preserving their price ratio. This test examines whether a higher capital cost changes storage size and the value obtained from peak shaving.

4.7.2 Fixed BESS duration

Fixed BESS duration is tested at 2, 3, 4, 5, and 6 h, with energy and power coupled by $E_B = T_B P_B$. Each value therefore represents a separate storage-duration configuration rather than only a tighter lower bound.

4.7.3 Daily EFC limit

The daily EFC limit is tested at 0.50, 0.75, 1.00, 1.25, and 1.50. This separates the allowed cycling level from that actually selected by the optimizer.

The flexible-duration baseline is shared by the cost and EFC groups, giving 14 unique settings in total. Each setting is run ten times with the two-stage RBMO. The Median and

interquartile range are emphasized because bus selection and stochastic search can make one best run unrepresentative.

4.8 Objective weight sensitivity

To investigate the effect of objective weights on the configuration scheme, seven cost/loss/voltage/peak weight vectors are selected: baseline (0.55, 0.15, 0.15, 0.15), equal (0.25, 0.25, 0.25, 0.25), lower cost weight (0.40, 0.20, 0.20, 0.20), higher cost weight (0.70, 0.10, 0.10, 0.10), loss priority (0.35, 0.35, 0.15, 0.15), voltage priority (0.35, 0.15, 0.35, 0.15), and peak priority (0.35, 0.15, 0.15, 0.35). Each setting is optimized through 30 matched-seed runs of the elite framework with 54210 search evaluations. The resulting physical indicators are compared to analyze the effects of weight selection, while fitness values obtained from different objectives are not ranked against each other.

4.9 Scaled operating conditions and transfer tests

Five operating conditions are constructed using the following pairs of load and PV scaling factors: nominal (1.00, 1.00), high load/low PV (1.15, 0.75), high load/high PV (1.15, 1.15), low load/low PV (0.85, 0.75), and low load/high PV (0.85, 1.15). In each pair, the first factor scales the load profile and the second scales the PV profile. The original temporal shapes are retained under these conditions, which do not represent the measured seasonal days or a model of PV-load correlation. For each condition, three assessment modes are employed: replanning, fixed nominal configuration with redispatch, and fixed nominal configuration with its original schedule. The comparative experiments therefore provide $5 \times 3 \times 30 = 450$ task records.

The search budget for each replanning run is set to 54210 evaluations. The 30 nominal replanning outputs are reused from the ablation experiment and verified, rather than counted as new independent runs. For a fixed configuration, the original schedule is evaluated once, and a random operation search is conducted with 12040 evaluations. The result with the lower penalized objective is retained, giving 12041 recorded evaluations. The fixed-schedule case requires one direct evaluation, and a separate no-equipment normalization reference is calculated for each condition. Nominal configurations are selected according to their run identifiers, rather than by selecting only favorable configuration schemes.

The redispatch acceptance mechanism retains a result with a penalized objective no greater than that of the incumbent under the same condition. However, feasibility-first dominance is not imposed by this mechanism. Therefore, constraint violations and feasible counts are reported separately from the accepted penalized objective. Failure to obtain a feasible operation scheme within the given search budget does not prove the mathematical infeasibility of the fixed configuration.

5. Results and Discussion

5.1 Engineering performance of the optimized PV-BESS system

Table 3 shows the Base, PV-only, and final PV-BESS cases. PV alone reduces economic cost from 50,591.69 to 33,439.02 CNY/day and peak grid power from 3917.68 to 2718.04 kW, showing that PV provides most of the energy substitution.

The final PV-BESS plan installs 3357.31 kW PV at buses 30 and 10 and a 1316.03 kWh/658.01 kW BESS at bus 28. Relative to Base, economic cost, energy loss, peak grid power, and voltage deviation decrease by 36.06, 32.96, 41.84, and 39.11%, respectively, while minimum voltage rises from 0.91309 to 0.94648 p.u. Terminal SOC is 0.5037, close to the initial 0.50.

Compared with PV-only, storage further reduces economic cost by 3.26% and peak grid power by 16.16%, although the additional loss reduction is only 0.75%. Thus, PV mainly replaces purchased energy, whereas BESS contributes more strongly to time shifting and peak control. The best run reaches the 2 h duration boundary and EFC = 1.0, so these limits are examined in Sect. 5.4 rather than treated as universal optima. The reported improvements assume accurate sensor inputs; measurement noise and communication delay are not simulated.

5.2 Equal-budget ablation and elite retention

Table 4 presents the final penalized objectives and feasibility results obtained from all 30 runs of each ablation method. Under the same search budget of 54210 evaluations, the mean objective obtained by the elite two-stage RBMO is 0.653401, which is reduced by 4.65% compared with the value of 0.685268 obtained by the direct single-stage RBMO. The corresponding medians are 0.655487 and 0.683008, respectively. In terms of the paired final-objective sign test, the elite framework obtains a lower value in 28 of 30 runs, with a Holm-adjusted p-value of 4.34×10^{-6} over the six-test family.

The mean final objective obtained without elite acceptance is 404.120545, while its median is 0.657703. This difference is due to a small number of runs with large penalty values, so the large mean does not represent an economic cost or a several-hundred-fold improvement in engineering

Table 3
Engineering comparison of Base, PV-only, and elite two-stage PV-BESS cases.

Indicator	Base	PV-only	Elite PV+BESS	PV+BESS vs Base
Fitness	1.000000	0.661696	0.630809	36.92% reduction
Total PV capacity (kW)	0	3100.42	3357.31	—
BESS energy (kWh) /power (kW)	—	—	1316.03/658.01	—
Grid energy (kWh)	64343.71	41615.22	39925.09	37.95% reduction
Energy loss (kWh)	2441.51	1649.14	1636.80	32.96% reduction
Peak grid power (kW)	3917.68	2718.04	2278.69	41.84% reduction
Voltage deviation	27.7952	17.1925	16.9244	39.11% reduction
Minimum voltage (p.u.)	0.91309	0.94054	0.94648	+0.03339 p.u.
Economic cost (CNY/day)	50591.69	33439.02	32348.11	36.06% reduction

Note: "—" indicates that the corresponding equipment is not included in the case or that the comparison is not applicable.

Table 4
Results of the equal-budget ablation experiment with 30 runs for each method and 54210 search evaluations for each run.

Method	Best	Mean	Median	SD	Feasible	Success	Time (s)
Single stage	0.653868	0.685268	0.683008	0.017814	30/30	2/30	38.82
Two-stage no elite	0.627975	404.120545	0.657703	1090.085828	24/30	15/30	38.54
Two-stage elite	0.630809	0.653401	0.655487	0.008665	28/30	25/30	38.51

Note: The objective statistics are calculated from all 30 final outputs. For the two-stage method without elite acceptance, the minimum objective of 0.627975 corresponds to an infeasible output, while the minimum objective among the feasible outputs is 0.635906.

performance. The feasible counts obtained by the single-stage RBMO, the two-stage RBMO without elite acceptance, and the two-stage RBMO with elite acceptance are 30/30, 24/30, and 28/30, respectively. However, the final-objective difference between the two-stage methods is not statistically significant after correction ($p = 0.303$). Therefore, Fig. 2 displays feasibility and penalized objective values separately.

In Table 4, a successful result needs to satisfy the feasibility criterion and have a fitness below 0.661696. The resulting success counts are 2/30, 15/30, and 25/30, respectively, while the earlier count of 27/30 for elite RBMO considered only the fitness threshold. For the feasible outputs, the mean final objectives are 0.685268, 0.660874, and 0.653934, respectively. These means describe different subsets and do not replace the paired analysis of all runs. The two infeasible elite outputs have terminal-SOC residuals of approximately 2.52×10^{-7} and 1.85×10^{-6} beyond the prescribed return band.

Across the 30 runs, 28 planning-stage and 49 operation-stage candidates are rejected by the elite framework. As illustrated by the stage means and medians in Fig. 3, the accepted objective does not increase between stages. In terms of the historical-best objective, the mean obtained without elite acceptance is 0.648570, which is lower than that obtained with elite acceptance (0.653401). However, not all historical-best candidates are feasible, with feasible counts of 25/30 and 28/30, respectively, and the historical-best difference between the two-stage methods is not statistically significant after correction ($p = 0.303$). Therefore, the results support the retention of accepted solution quality, but do not establish an improvement in global exploration through elite acceptance.

5.3 Comparison with alternative optimizers

Under the aligned evaluation budget, no optimizer dominates every indicator (Table 5). GWO has the lowest mean and median fitness, GA the lowest single best value, RBMO the smallest standard deviation, and PSO the shortest mean runtime by a small margin.

The stored complete outputs of the historical benchmark are rechecked using the same residual tolerance of 10^{-7}. The feasible count of RBMO is 28/30, while those of PSO, GWO, and GA are 30/30. In Table 5, success requires both feasibility and a fitness below 0.661696, giving 25/30 successful runs for RBMO and 30/30 for the other methods. The original fitness distributions and non-parametric tests are retained without change.

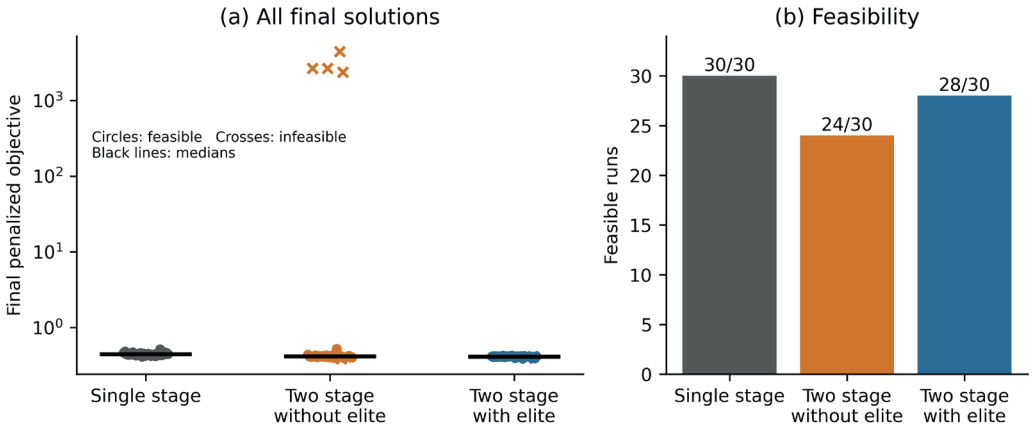

Fig. 2. (Color online) Results of the equal-budget ablation experiment. Circles, crosses, and black segments represent feasible final outputs, infeasible outputs, and medians, respectively. The objective axis is linear up to 1 and logarithmic above this value to display the runs with large penalties, while feasible counts are presented separately.

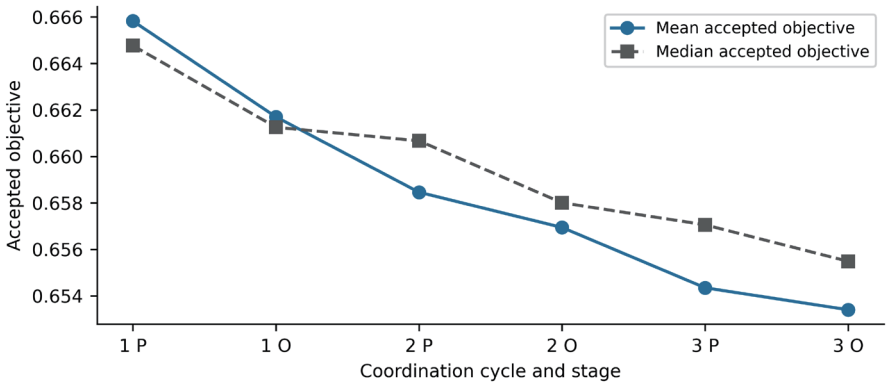

Fig. 3. (Color online) Mean and median accepted objective values obtained after the planning stage P and operation stage O in each cycle of the elite framework. Each point represents the results of the same 30 runs.

Table 5
Thirty-run comparison under aligned objective-function evaluation budgets.

Method	Best	Mean	Median	SD	Feasible	Success	Time (s)
RBMO	0.630809	0.653401	0.655487	0.008665	28/30	25/30	37.44
PSO	0.614425	0.644976	0.654872	0.016891	30/30	30/30	36.84
GWO	0.616182	0.639179	0.641303	0.016336	30/30	30/30	59.92
GA	0.614244	0.642447	0.649814	0.017212	30/30	30/30	72.72

Figure 4 illustrates the fitness distributions obtained by the four optimizers in the historical comparison. The mean fitness obtained by GWO is 0.639179, which is reduced by 2.18% compared with the RBMO mean fitness of 0.653401. PSO and GA also obtain lower mean values, while RBMO has the smallest reported standard deviation of 0.008665. The historical benchmark is retained as a separate experiment, and its outputs are not combined with the revised ablation results because the single-stage reference and evaluation-accounting conventions are different.

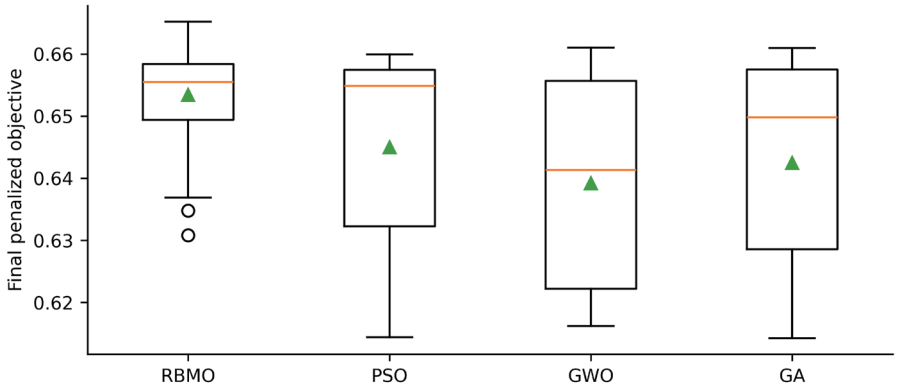

Fig. 4. (Color online) Distributions of the historical final objectives obtained by RBMO, PSO, GWO, and GA under aligned evaluation budgets. Boxes span Q1–Q3, center lines represent medians, triangles represent means, whiskers follow the 1.5-IQR rule, and circles represent outliers.

The Kruskal-Wallis test gives $H = 11.911$ and $p = 0.00769$. After Holm correction, RBMO differs significantly from GWO ($p = 0.00141$) and GA ($p = 0.04649$), while the PSO difference is not significant ($p = 0.0850$). Positive Cliff's delta values indicate that RBMO tends to return higher fitness in the significant comparisons (Table 6).

Accordingly, the results do not support universal RBMO superiority. RBMO is used here as the main engine for demonstrating the planning-operation framework, and its advantage is lower dispersion. The successful use of PSO, GWO, and GA also indicates that the framework is not tied to one population-update rule.

5.4 Sensitivity analysis

Sensitivity results are interpreted from ten-run medians and interquartile ranges rather than one best solution.

5.4.1 BESS investment-cost sensitivity

Figure 5 shows the effects of BESS investment cost on the optimized configuration scheme. When the cost multiplier increases from 0.6 to 1.4, the median fitness increases overall from 0.645715 to 0.658298. A lower investment cost also produces a greater reduction in peak power, but the selected storage capacity does not change monotonically at every setting. This variation may be related to discrete bus selection and stochastic optimization, so the results indicate a general cost-performance tendency rather than a deterministic relationship between price and capacity.

5.4.2 Daily EFC-limit sensitivity

Figure 6 illustrates the operation results obtained under different daily-EFC limits. The actual EFC follows the limits of 0.50 and 0.75, and reaches 1.243 when the limit is set to 1.25.

Table 6
Non-parametric comparison of RBMO with the benchmark optimizers.

Comparison	U	Raw p	Holm p	Cliff's δ	Interpretation
RBMO vs PSO	567	0.0850	0.0850	+0.260	Not significant
RBMO vs GWO	687	0.000471	0.00141	+0.527	GWO better
RBMO vs GA	604	0.02324	0.04649	+0.342	GA better

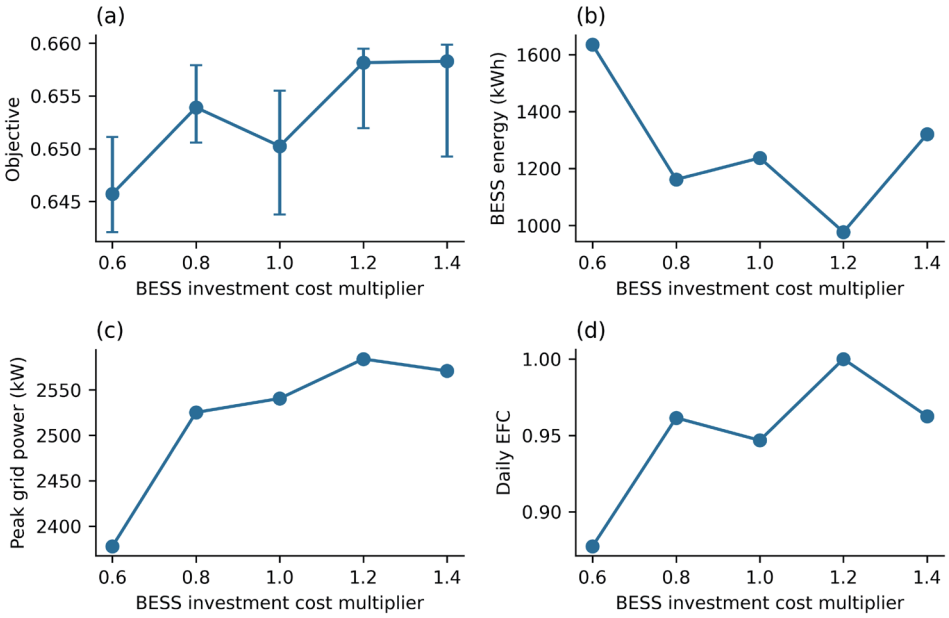

Fig. 5. (Color online) Effects of BESS investment cost on the optimization results. Each point represents the median of ten runs. The objective error bars span Q1–Q3, while the other panels present medians without error bars.

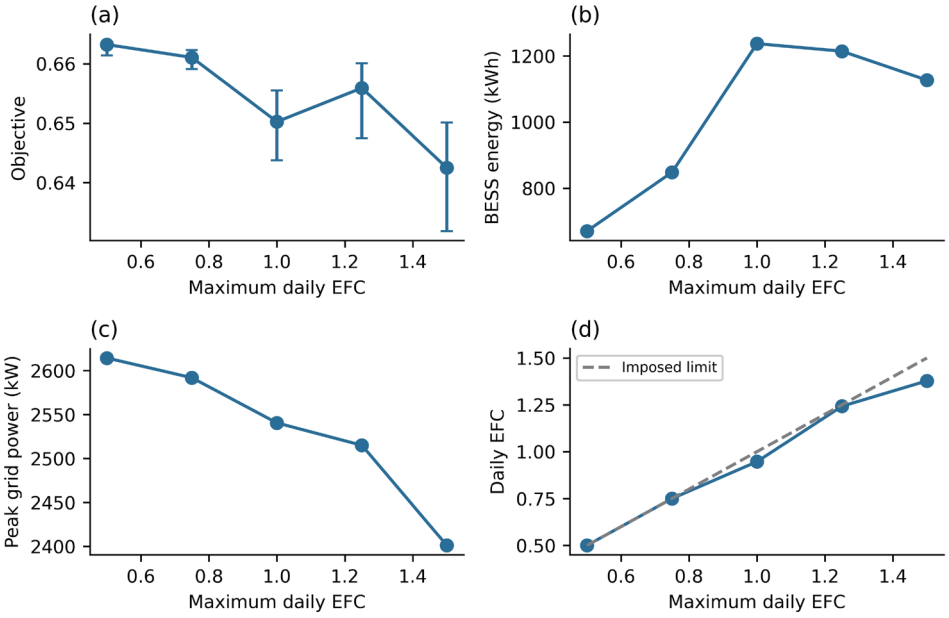

Fig. 6. (Color online) Effects of the daily-EFC limit on the optimization results. Each point represents the median of ten runs, and objective error bars span Q1–Q3. The dashed line in the EFC panel represents the imposed limit.

However, when the allowed EFC is 1.50, the actual value is only 1.378. Between the two endpoints, the median peak grid power decreases from 2614.34 to 2401.05 kW, and the median fitness decreases from 0.663229 to 0.642492. Therefore, increasing the permitted cycling level provides additional operation flexibility, but the optimized scheme does not necessarily use the full cycling allowance.

5.4.3 Fixed BESS-duration sensitivity

Figure 7 presents the optimized results obtained under different fixed BESS durations. When the duration increases from 2 to 6 h, the median fitness decreases from 0.656536 to 0.644249, and the median BESS energy increases from 370.56 to 2114.36 kWh. At 6 h, the peak grid power is reduced to 2397.95 kW, while the 6 h case has a median EFC of 0.772, indicating that the improvement is related to a larger energy reservoir rather than more frequent cycling. However, this setting is only the best duration among the tested values and is not established as a global duration optimum.

5.5 Objective weight trade-offs

Table 7 displays the physical indicators obtained from all 30 outputs under different weight settings, and the feasible counts are presented separately. In terms of economy, the higher economic weight obtains the lowest mean cost. In terms of network performance, loss priority, peak priority, and voltage priority obtain the lowest mean energy loss, mean peak power, and

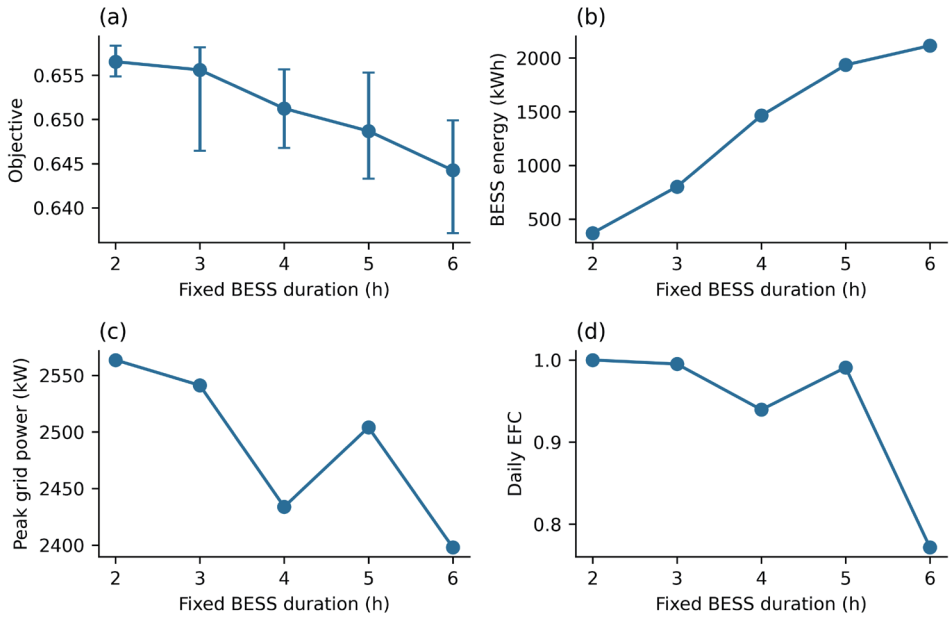

Fig. 7. (Color online) Effects of fixed BESS duration on the optimization results. Each point represents the median of ten runs. The objective error bars span Q1–Q3, while the other panels present medians without error bars.

Table 7
Optimization results obtained under different objective weights with 30 runs for each setting.

Weights	Cost (CNY/day)	Loss (kWh/day)	Peak (kW)	Voltage deviation	Feasible
Baseline	33403	1651	2511	17.177	28/30
Cost high	33289	1657	2527	17.220	28/30
Cost low	33376	1642	2479	17.190	28/30
Equal	33498	1644	2469	17.171	28/30
Loss priority	33408	1621	2468	17.391	29/30
Peak priority	33518	1646	2463	17.244	24/30
Voltage priority	33404	1661	2488	16.996	29/30

accumulated voltage deviation, respectively, among the tested settings. These results describe the finite-run comparison and do not constitute a statistical ranking of stakeholder preferences. Since the voltage objective accumulates deviation over buses and hours, a greater voltage weight does not necessarily improve the minimum voltage.

The mean values are calculated from all returned outputs, and the infeasible outputs are not considered deployable configuration schemes. The corresponding feasible-only summaries are provided separately, and the weight vectors are given in Sect. 4.8.

Figure 8 shows the means of all outputs and feasible outputs to illustrate the effect of using different subsets. Figure 9 shows the BESS capacities obtained under different weight settings. The mean BESS energy/power changes from 1121/413 kWh/kW at baseline to 1619/702 under peak priority and 1679/693 under equal weights, indicating that the selected capacities depend materially on the planning preference. Since bus selection is discrete, the siting frequencies are also provided in the supplementary data. The number of feasible runs ranges from 24 to 29 for each setting, and the infeasible results arise from small terminal-SOC or EFC residuals under the unchanged classification rule.

5.6 Operating conditions and nominal-plan transfer

Table 8 and Fig. 10 show the results obtained by replanning for each condition and operating a nominal configuration under that condition. The feasible counts obtained through replanning are 28/30, 28/30, 29/30, 28/30, and 30/30 under nominal, high-load/low-PV, high-load/high-PV, low-load/low-PV, and low-load/high-PV conditions, respectively. The infeasible replanning results are caused by small terminal-SOC or EFC residuals, and the replanned outputs have no voltage or export violations.

The residual tolerance is maintained at 10^{-7} for all classifications. The original 30 configurations are reused for nominal replanning, and the redispatch mechanism selects the result with the lower penalized objective rather than applying a feasibility-first rule.

Under low load and high PV, the feasible counts of both fixed-plan groups are 0/30, while the feasible count obtained by replanning is 30/30. Redispatch reduces the mean penalized objective from 18117.87 to 14228.01, but the retained operation schemes still violate the no-export requirement. These objective values are dominated by penalties and do not represent economic costs or feasible operation benefits. The maximum recorded export residual after redispatch is 1088.20 kW. Since the selection criterion minimizes the total penalized objective rather than the

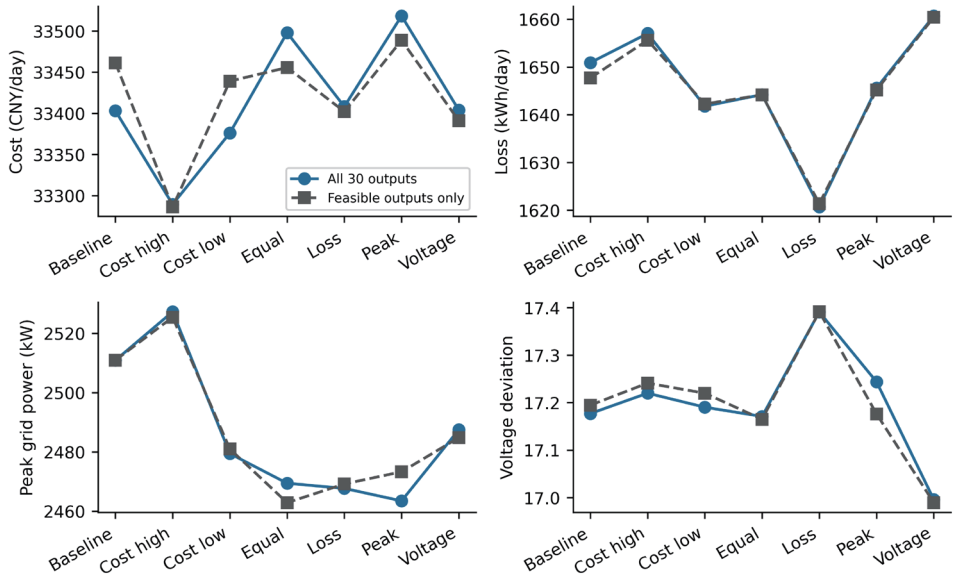

Fig. 8. (Color online) Physical objective indicators obtained under seven weight settings. Solid lines represent the means of all 30 outputs, while dashed lines represent the means of feasible outputs only.
The different subset sizes are given in Table 7.

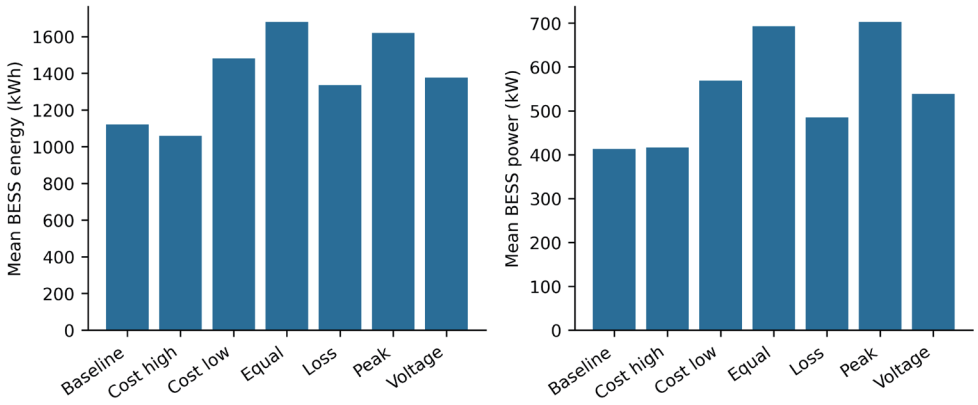

Fig. 9. (Color online) Mean BESS energy and power obtained from all 30 outputs under each weight setting. The corresponding feasible counts are given in Table 7.

Table 8
Feasible results obtained under five scaled operating conditions.

Condition	Load/PV scale	Replan	Fixed plan redispatch	Fixed plan schedule
Nominal	1.00/1.00	28/30	28/30	28/30
High load low PV	1.15/0.75	28/30	27/30	28/30
High load high PV	1.15/1.15	29/30	27/30	24/30
Low load low PV	0.85/0.75	28/30	28/30	28/30
Low load high PV	0.85/1.15	30/30	0/30	0/30

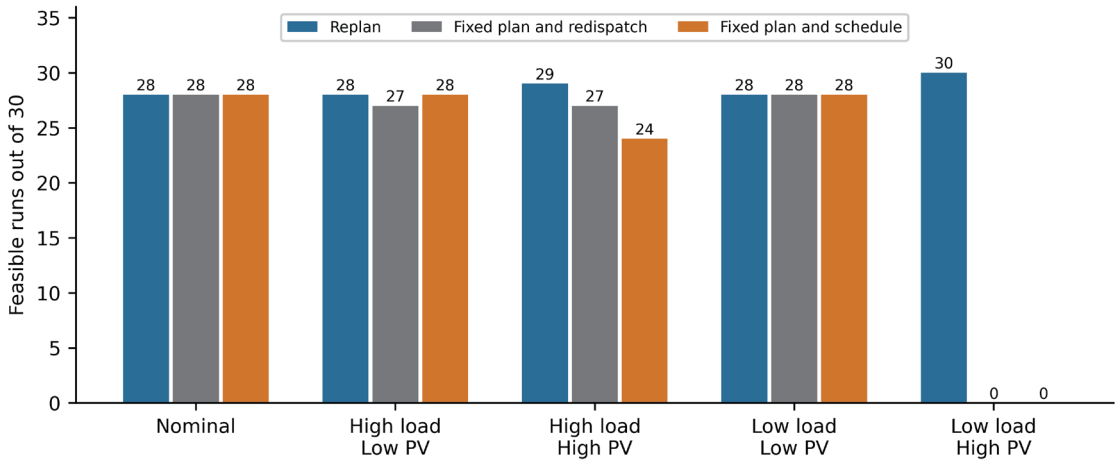

Fig. 10. (Color online) Feasible outputs obtained from 30 runs under each condition and assessment mode. The nominal replanning outputs are reused from the ablation experiment.

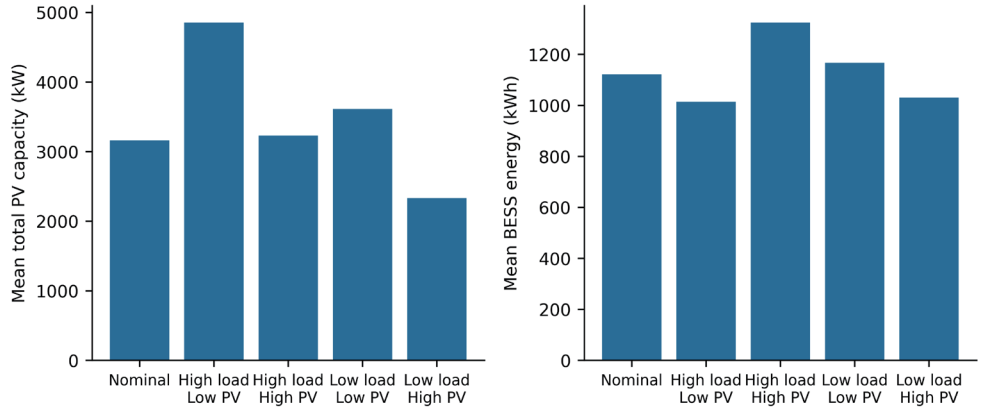

Fig. 11. (Color online) Mean total PV capacity and BESS energy obtained from 30 condition-specific replanning outputs. The corresponding feasible counts are presented separately in Table 8.

largest individual residual, this maximum does not necessarily decrease compared with the fixed-schedule result.

For high-load/high-PV conditions, the feasible count increases from 24/30 to 27/30 after redispatch. Under high-load/low-PV conditions, the count changes from 28/30 to 27/30. The latter result is consistent with the penalty-based acceptance mechanism, indicating that the non-deterioration of the objective should be reported together with feasibility. The original schedules are retained in 78 of the 150 fixed-plan tasks, including 21 of 30 tasks under nominal conditions, so random redispatch is prevented from worsening the objective.

Figure 11 illustrates the differences in PV and storage capacities obtained by replanning under different operating conditions. The results indicate the need to consider multiple correlated conditions in the planning model, but independently optimizing each condition does not establish a single robust annual configuration scheme. In addition, the tests do not preserve

realistic seasonal correlations and do not provide certificates of infeasibility for the fixed nominal configurations.

6. Conclusion

In this study, a planning-operation framework is constructed by combining decomposition, a common repaired objective, and an inter-stage elite acceptance mechanism, while the original RBMO update rules are retained. Under the equal-budget comparison with 30 runs, the elite framework reduces the mean penalized objective by 4.65% compared with the single-stage RBMO. The elite mechanism prevents the deterioration of the shared state, but its difference from the two-stage method without elite acceptance is not statistically significant, and an improvement in global search is not established. In addition, the weight sensitivity results show that the selected storage ratings depend on the planning preference. Under low-load/high-PV conditions, replanning obtains 30/30 feasible outputs, while the fixed nominal configurations obtain 0/30 feasible outputs within the tested redispatch budget. Therefore, the scaled-condition tests reveal the limitation of single-day designs, rather than establishing annual feasibility or uncertainty robustness. The measured profiles provide the relation to sensing applications, while voltage and SOC are simulated and are not independently sensed or field-validated. For practical deployment, synchronized multi-day measurements, sensor error, communication delay, and correlated operating conditions need to be considered. In future research, the model can be further extended by introducing PV curtailment, inverter reactive support, and more detailed battery-aging models.

References

1 Y. Wang and J. Wu: Int. J. Electr. Power Energy Syst. **167** (2025) 110654. https://doi.org/10.1016/j.ijepes.2025.110654
2 K. Shinde and P. B. Mane: Energy Rep. **8** (2022) 5852. https://doi.org/10.1016/j.egyr.2022.03.086
3 H. S. Zhou, R. Passey, A. Bruce, and A. B. Sproul: J. Energy Storage **52** (2022) 104817. https://doi.org/10.1016/j.est.2022.104817
4 D. Zhang, G. M. Shafiullah, C. K. Das, and K. W. Wong: J. Energy Storage **56** (2022) 105937. https://doi.org/10.1016/j.est.2022.105937
5 P. Boonluk, A. Siritaratiwat, P. Fuangfoo, and S. Khunkitti: Batteries **6** (2020) 56. https://doi.org/10.3390/batteries6040056
6 A. Inaolaji, X. Wu, R. Roychowdhury, and R. Smith: J. Energy Storage **95** (2024) 112305. https://doi.org/10.1016/j.est.2024.112305
7 C. Jamroen: Electr. Power Syst. Res. **211** (2022) 108340. https://doi.org/10.1016/j.epsr.2022.108340
8 R. Chedid and A. Sawwas: Energy Storage **1** (2019) e46. https://doi.org/10.1002/est2.46
9 R. A. Thokar, N. Gupta, K. R. Niazi, A. Swarnkar, and N. K. Meena: J. Energy Storage **35** (2021) 102263. https://doi.org/10.1016/j.est.2021.102263
10 M. A. Elseify, A. SeyyedAbbasi, J. L. Domínguez-García, and S. Kamel: J. Energy Storage **73** (2023) 108986. https://doi.org/10.1016/j.est.2023.108986
11 M. A. Elseify, R. R. Mostafa, F. A. Hashim, J. L. Domínguez-García, and S. Kamel: J. Energy Storage **116** (2025) 116026. https://doi.org/10.1016/j.est.2025.116026
12 P. Qiu, H. Guo, J. Zhang, X. Bai, L. Yan, and Z. Ullah: Results Eng. **30** (2026) 110919. https://doi.org/10.1016/j.rineng.2026.110919
13 Y. Ji, X. Zhang, P. He, S. Wang, X. Liu, and C. Li: Electr. Power Syst. Res. **252** (2026) 112383. https://doi.org/10.1016/j.epsr.2025.112383

14 V. Saxena, S. K. Rajput, S. Manna, A. Gantayet, K. L. Agarwal, M. H. Alsharif, and M. -K. Kim: Energy Rep. **15** (2026) 108882. https://doi.org/10.1016/j.egyr.2025.12.019
15 B. Cortés-Caicedo, O. D. Montoya, L. F. Grisales-Noreña, E. E. Gaona-García, and J. Ardila-Rey: J. Energy Storage **123** (2025) 116639. https://doi.org/10.1016/j.est.2025.116639
16 M. Wang, F. Zhang, L. Zhang, J. Chen, and B. Zhao: J. Energy Storage **172** (2026) 122980. https://doi.org/10.1016/j.est.2026.122980
17 L. Yang, J. Teh, and B. Alharbi: J. Energy Storage **91** (2024) 111989. https://doi.org/10.1016/j.est.2024.111989
18 J. Carrasco, S. García, M. M. Rueda, S. Das, and F. Herrera: Swarm Evol. Comput. **54** (2020) 100665. https://doi.org/10.1016/j.swevo.2020.100665
19 V. Beiranvand, W. Hare, and Y. Lucet: Optim. Eng. **18** (2017) 815. https://doi.org/10.1007/s11081-017-9366-1
20 S. Fu, K. Li, H. Huang, C. Ma, Q. Fan, and Y. Zhu: Artif. Intell. Rev. **57** (2024) 134. https://doi.org/10.1007/s10462-024-10716-3
21 P. Tseng: J. Optim. Theory Appl. **109** (2001) 475. https://doi.org/10.1023/A:1017501703105
22 M. E. Baran and F. F. Wu: IEEE Trans. Power Delivery **4** (1989) 1401. https://doi.org/10.1109/61.25627
23 C. Schade and R. Egging-Bratseth: Energy Storage **6** (2024) e588. https://doi.org/10.1002/est2.588